JOURNAL OF GUIDANCE, CONTROL, AND DYNAMICS
Vol. 23, No. 3, May–June 2000

Adaptive Nonlinear Control of Multiple Spacecraft Formation Flying

Marcio S. de Queiroz,* Vikram Kapila,† and Qiguo Yan‡
Polytechnic University, Brooklyn, New York 11201

This paper considers the problem of relative position control for multiple spacecraft formation flying. Specifically, the full nonlinear dynamics describing the relative positioning of multiple spacecraft formation flying are used to develop a Lyapunov-based, nonlinear, adaptive control law that guarantees global asymptotic convergence of the position tracking error in the presence of unknown, constant, or slow-varying spacecraft masses, disturbance forces, and gravity forces. Simulation results are included to illustrate the controller performance.

I. Introduction

MULTIPLE spacecraft formation flying (MSFF) represents the concept of distributing the functionality of large spacecraft among smaller, less-expensive, cooperative spacecraft.[1,2] Specifically, NASA and the U.S. Air Force have identified spacecraft formation flying as an enabling technology for future missions and have shown a keen interest in the development of a reliable, autonomous, formation keeping strategy to deploy multiple spacecraft for space missions, e.g., the Earth Orbiter-I (EO-I) and the New Millennium Interferometer (NMI), also known as Deep Space-3. This interest has led to several studies on autonomous MSFF being reported in the literature. For example, in early research Ref. 3 presented the concept of formation keeping of spacecraft for a ground-based terrestrial laser communication system, whereas Ref. 4 considered station keeping for the Space Shuttle Orbiter. Recently, Ref. 5 considered MSFF control for NASA's NMI mission using separated spacecraft interferometry. Similarly, Ref. 6 considered MSFF control for NASA's EO-I mission, which is scheduled to demonstrate a stereo imaging concept in 1999.

The practical implementation of the MSFF concept relies on the accurate control of the relative positions and orientations between the participating spacecraft for formation configuration and collision avoidance. Most MSFF control designs use simplifying modeling assumptions to aid the control synthesis caused by inherent difficulties associated with the structure of the full, nonlinear dynamic model of MSFF. These simplifications result in the well-known Clohessy–Wiltshire linear, dynamic equations[7–9] for the relative positioning of MSFF. The Clohessy–Wiltshire model has formed the basis for the application of various linear control techniques to the MSFF position control problem.[3,4,9,10] Reviewing the current state of MSFF control, it seems that in contrast to linear control nonlinear control theory has not been exploited to its full potential in MSFF. To the best of our knowledge, one of the few results on nonlinear control of MSFF can be found in Refs. 11–13 using a Lyapunov-based approach. In particular, Ref. 12 designed a class of control laws based on exact knowledge of the MSFF model that yielded local asymptotic position tracking and global exponential attitude tracking. The application of the controllers proposed in Ref. 12 to formation rotation of MSFF about a given axis and synchronization of individual spacecraft rotation was later reported in Ref. 13. More recently, Ref. 11 developed an adaptive position controller that compensated for unknown, constant disturbances while producing globally asymptotically decaying position tracking errors. This controller, however, required exact knowledge of the spacecraft parameters.

In this paper we consider the full nonlinear dynamics describing the relative positioning of MSFF for control design purposes. Using Lyapunov-based control design and stability analysis techniques, we develop a nonlinear adaptive control law that guarantees global asymptotic convergence of the spacecraft relative position to any sufficiently smooth desired trajectory, despite the presence of unknown, constant, or slow-varying spacecraft masses, disturbance forces, and gravity forces. In the case when the parameters are exactly known, the proposed control strategy yields global exponential convergence of the tracking errors. In comparison to the work of Refs. 11 and 12, the proposed controller ensures stronger stability results and accounts for a wider class of parametric uncertainties. As in Refs. 11–13, we will consider in this paper the idealized scenario where the spacecraft actuators are capable of providing continuous-time control efforts, as opposed to being of pulse type.[9] We note that the problem of pulse-type, nonlinear control design for MSFF constitutes an open research problem and is beyond the scope of this paper.

The paper is organized as follows. Section II presents the nonlinear dynamic model derivation. The control objective is stated in Sec. III. The control design and closed-loop stability analysis are presented in Sec. IV. Simulation results are provided in Sec. V, whereas some concluding remarks are given in Sec. VI.

II. System Model

In this section we present the derivation of a nonlinear MSFF system model in a form that facilitates the subsequent design and stability analysis of the nonlinear, Lyapunov-based control law. In the modeling that follows, we consider each spacecraft to be a point-mass evolving in free space. We assume the MSFF fleet is composed of two spacecraft, i.e., a *leader* spacecraft that provides the basic reference motion trajectory and a *follower* spacecraft that navigates in the neighborhood of the leader spacecraft according to a desired, relative trajectory. Furthermore, we assume that the leader spacecraft is in a circular orbit around the Earth with constant angular velocity ω. The preceding assumption has been made for the ease of presentation. The control design framework of this paper can be easily extended to the case where one considers an arbitrary (possibly non-Keplarian) motion of the leader spacecraft.

A schematic drawing of the MSFF system is depicted in Fig. 1, where we make the following considerations: 1) the inertial coordinate system $\{X, Y, Z\}$ is attached to the center of the Earth, 2) $\boldsymbol{R}(t) \in \mathbb{R}^3$ denotes the position vector from the origin of the inertial coordinate system to the leader spacecraft, 3) the coordinate system $\{x_\ell, y_\ell, z_\ell\}$ is attached to the leader spacecraft with the x_ℓ axis pointing in the opposite direction as the tangential velocity, the y_ℓ axis pointing along the direction of the vector $\boldsymbol{R}$, and the z_ℓ axis being mutually perpendicular to the x_ℓ and y_ℓ axes such that

Received 3 June 1999; presented as Paper 99-4270 at the AIAA Guidance, Navigation, and Control Conference, Portland, OR, 9–11 August 1999; revision received 8 October 1999; accepted for publication 24 October 1999.

*Assistant Professor, Department of Mechanical, Aerospace, and Manufacturing Engineering, 6 Metrotech Center; queiroz@poly.edu.
†Assistant Professor, Department of Mechanical, Aerospace, and Manufacturing Engineering, 6 Metrotech Center; vkapila@poly.edu.
‡Graduate Student, Department of Mechanical, Aerospace, and Manufacturing Engineering, 6 Metrotech Center; qyan01@utopia.poly.edu.

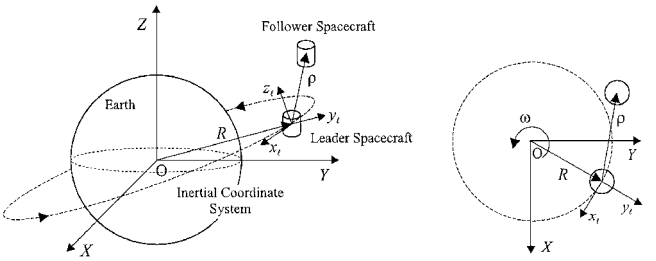

Fig. 1 Schematic representation of the MSFF system.

$\{x_\ell, y_\ell, z_\ell\}$ forms a right-hand coordinate frame, and 4) $\boldsymbol{\rho}(t) \in \mathbb{R}^3$ denotes the relative position vector from the origin of the leader spacecraft coordinate system to the follower spacecraft.

The nonlinear position dynamics of the leader and follower spacecraft with respect to the inertial coordinate system $\{X, Y, Z\}$ are given by[3,9]

$$m_\ell \ddot{\boldsymbol{R}} + m_\ell(M + m_\ell)G(\boldsymbol{R}/\|\boldsymbol{R}\|^3) + \boldsymbol{F}_{d\ell} = \boldsymbol{u}_\ell \tag{1}$$

and

$$m_{\mathrm{f}}(\ddot{\boldsymbol{R}} + \ddot{\boldsymbol{\rho}}) + m_{\mathrm{f}}(M + m_{\mathrm{f}})G\frac{\boldsymbol{R} + \boldsymbol{\rho}}{\|\boldsymbol{R} + \boldsymbol{\rho}\|^3} + \boldsymbol{F}_{\mathrm{df}} = \boldsymbol{u}_{\mathrm{f}} \tag{2}$$

respectively, where m_ℓ, m_{f} are the masses; $\boldsymbol{F}_{d\ell}, \boldsymbol{F}_{\mathrm{df}} \in \mathbb{R}^3$ are disturbance force vectors and $\boldsymbol{u}_\ell(t), \boldsymbol{u}_{\mathrm{f}}(t) \in \mathbb{R}^3$ are the actual control input vectors of the leader and follower spacecraft, respectively; M is the Earth's mass; and G is the universal gravity constant. Because $M \gg m_\ell$, m_{f}, Eqs. (1) and (2) can be simplified to the following equations:

$$m_\ell \ddot{\boldsymbol{R}} + m_\ell MG(\boldsymbol{R}/\|\boldsymbol{R}\|^3) + \boldsymbol{F}_{d\ell} = \boldsymbol{u}_\ell \tag{3}$$

and

$$m_{\mathrm{f}}(\ddot{\boldsymbol{R}} + \ddot{\boldsymbol{\rho}}) + m_{\mathrm{f}}MG\frac{\boldsymbol{R} + \boldsymbol{\rho}}{\|\boldsymbol{R} + \boldsymbol{\rho}\|^3} + \boldsymbol{F}_{\mathrm{df}} = \boldsymbol{u}_{\mathrm{f}} \tag{4}$$

respectively. After some simple algebraic manipulations on Eqs. (3) and (4), the dynamic equation describing the position of the follower spacecraft relative to the leader spacecraft in the coordinate system $\{X, Y, Z\}$ can be written as

$$m_{\mathrm{f}}\ddot{\boldsymbol{\rho}} + m_{\mathrm{f}}MG\left(\frac{\boldsymbol{R} + \boldsymbol{\rho}}{\|\boldsymbol{R} + \boldsymbol{\rho}\|^3} - \frac{\boldsymbol{R}}{\|\boldsymbol{R}\|^3}\right) + \frac{m_{\mathrm{f}}}{m_\ell}\boldsymbol{u}_\ell + \boldsymbol{F}_{\mathrm{df}} - \frac{m_{\mathrm{f}}}{m_\ell}\boldsymbol{F}_{d\ell} = \boldsymbol{u}_{\mathrm{f}} \tag{5}$$

Remark 1: In the preceding model we consider that the spacecraft masses vary slowly in time because of fuel consumption and payload variations. Furthermore, we consider that the disturbance forces result from solar radiation, aerodynamics, and magnetic fields, and, hence, are also slow time-varying quantities.[11] As such, we can assume m_ℓ, m_{f} are constant parameters and $\boldsymbol{F}_{d\ell}, \boldsymbol{F}_{\mathrm{df}}$ are constant vectors.

To write the dynamics of Eq. (5) in terms of the moving coordinate system $\{x_\ell, y_\ell, z_\ell\}$, first notice that the relative position vector $\boldsymbol{\rho}(t)$ expressed in $\{x_\ell, y_\ell, z_\ell\}$ is given by

$$\boldsymbol{\rho} = x\hat{\boldsymbol{\imath}}_\ell + y\hat{\boldsymbol{\jmath}}_\ell + z\hat{\boldsymbol{k}}_\ell \tag{6}$$

where $\hat{\boldsymbol{\imath}}_\ell, \hat{\boldsymbol{\jmath}}_\ell, \hat{\boldsymbol{k}}_\ell$ denote the unit vectors, while the constant angular velocity $\boldsymbol{\omega}$ is given by $\omega\hat{\boldsymbol{k}}_\ell$. Hence, the relative acceleration vector $\ddot{\boldsymbol{\rho}}(t)$ is given by

$$\ddot{\boldsymbol{\rho}} = (\ddot{x} - 2\omega\dot{y} - \omega^2 x)\hat{\boldsymbol{\imath}}_\ell + (\ddot{y} + 2\omega\dot{x} - \omega^2 y)\hat{\boldsymbol{\jmath}}_\ell + \ddot{z}\hat{\boldsymbol{k}}_\ell \tag{7}$$

Furthermore, in the moving coordinate system $\{x_\ell, y_\ell, z_\ell\}$ the vector $\boldsymbol{R} = \|\boldsymbol{R}\|\hat{\boldsymbol{\jmath}}_\ell$ and is constant. After substituting the right-hand side of Eq. (7) into Eq. (5), the nonlinear position dynamics of the follower spacecraft relative to the leader spacecraft can be arranged into the following advantageous form:

$$m_{\mathrm{f}}\ddot{\boldsymbol{q}} + C(\omega)\dot{\boldsymbol{q}} + N(\boldsymbol{q}, \omega, \boldsymbol{R}, \boldsymbol{u}_\ell) + \boldsymbol{F}_{\mathrm{d}} = \boldsymbol{u}_{\mathrm{f}} \tag{8}$$

where the relative position vector $\boldsymbol{q}(t) \in \mathbb{R}^3$

$$\boldsymbol{q}(t) \triangleq [x(t) \quad y(t) \quad z(t)]^T \tag{9}$$

$C(\omega) \in \mathbb{R}^{3\times 3}$ is the Coriolis-like matrix given by

$$C(\omega) \triangleq 2m_{\mathrm{f}}\omega\begin{bmatrix} 0 & -1 & 0 \\ 1 & 0 & 0 \\ 0 & 0 & 0 \end{bmatrix} \tag{10}$$

$\boldsymbol{N}(\cdot) \in \mathbb{R}^3$ is a nonlinear term defined as

$$\boldsymbol{N}(\boldsymbol{q}, \omega, \boldsymbol{R}, \boldsymbol{u}_\ell) \triangleq \begin{bmatrix} m_{\mathrm{f}}MG\dfrac{x}{\|\boldsymbol{R} + \boldsymbol{q}\|^3} - m_{\mathrm{f}}\omega^2 x + \dfrac{m_{\mathrm{f}}}{m_\ell}u_{\ell_x} \\ m_{\mathrm{f}}MG\left(\dfrac{y + \|\boldsymbol{R}\|}{\|\boldsymbol{R} + \boldsymbol{q}\|^3} - \dfrac{1}{\|\boldsymbol{R}\|^2}\right) - m_{\mathrm{f}}\omega^2 y + \dfrac{m_{\mathrm{f}}}{m_\ell}u_{\ell_y} \\ m_{\mathrm{f}}MG\dfrac{z}{\|\boldsymbol{R} + \boldsymbol{q}\|^3} + \dfrac{m_{\mathrm{f}}}{m_\ell}u_{\ell_z} \end{bmatrix} \tag{11}$$

with $u_{\ell_x}(t), u_{\ell_y}(t), u_{\ell_z}(t)$ being the components of the leader control input vector $\boldsymbol{u}_\ell(t)$ and $\boldsymbol{F}_{\mathrm{d}} \in \mathbb{R}^3$ is the total, constant disturbance force vector given by

$$\boldsymbol{F}_{\mathrm{d}} \triangleq \boldsymbol{F}_{\mathrm{df}} - (m_{\mathrm{f}}/m_\ell)\boldsymbol{F}_{\mathrm{d}\ell} \tag{12}$$

The dynamic model of Eqs. (8–12) has the following property, which will be exploited in the subsequent adaptive control design. The left-hand side of the dynamic equation (8) can be linearly parameterized as

$$m_{\mathrm{f}}\boldsymbol{\xi} + C(\omega)\dot{\boldsymbol{q}} + \boldsymbol{N}(\boldsymbol{q}, \omega, \boldsymbol{R}, \boldsymbol{u}_\ell) + \boldsymbol{F}_d = W(\boldsymbol{\xi}, \dot{\boldsymbol{q}}, \boldsymbol{q}, \omega, \boldsymbol{R}, \boldsymbol{u}_\ell)\boldsymbol{\theta} \tag{13}$$

where $\boldsymbol{\xi} \in \mathbb{R}^3$ is a dummy variable, $W(\cdot) \in \mathbb{R}^{3\times 6}$ is the regression matrix that is composed of known functions, and $\boldsymbol{\theta} \in \mathbb{R}^6$ is the system's constant parameter vector. From the form of Eqs. (8–12), it is not difficult to see that $W(\cdot)$ and $\boldsymbol{\theta}$ can be explicitly defined as follows:

$$W(\boldsymbol{\xi}, \dot{\boldsymbol{q}}, \boldsymbol{q}, \omega, \boldsymbol{R}, \boldsymbol{u}_\ell) \triangleq \begin{bmatrix} \xi_x - 2\omega\dot{y} - \omega^2 x & \dfrac{x}{\|\boldsymbol{R} + \boldsymbol{q}\|^3} & u_{\ell_x} & 1 & 0 & 0 \\ \xi_y + 2\omega\dot{x} - \omega^2 y & \dfrac{y + \|\boldsymbol{R}\|}{\|\boldsymbol{R} + \boldsymbol{q}\|^3} - \dfrac{1}{\|\boldsymbol{R}\|^2} & u_{\ell_y} & 0 & 1 & 0 \\ \xi_z & \dfrac{z}{\|\boldsymbol{R} + \boldsymbol{q}\|^3} & u_{\ell_z} & 0 & 0 & 1 \end{bmatrix} \tag{14}$$

and

$$\boldsymbol{\theta} \triangleq [m_{\mathrm{f}} \quad m_{\mathrm{f}}MG \quad m_{\mathrm{f}}/m_\ell \quad F_{\mathrm{dx}} \quad F_{\mathrm{dy}} \quad F_{\mathrm{dz}}]^T \tag{15}$$

where ξ_x, ξ_y, ξ_z and $F_{\mathrm{dx}}, F_{\mathrm{dy}}, F_{\mathrm{dz}}$ are the components of the vectors $\boldsymbol{\xi}$ and $\boldsymbol{F}_{\mathrm{d}}$, respectively.

III. Control Objective

Given a desired position trajectory $\boldsymbol{q}_{\mathrm{d}}(t) \in \mathbb{R}^3$ for the follower spacecraft with respect to the leader spacecraft [we assume that $\boldsymbol{q}_{\mathrm{d}}(t)$ and its first two time derivatives are all bounded functions of time], the primary objective of MSFF is to design the control input $\boldsymbol{u}_{\mathrm{f}}(t)$ such that $\boldsymbol{q}(t) \to \boldsymbol{q}_{\mathrm{d}}(t)$ as $t \to \infty$. This objective is to be met with the assumption that $\boldsymbol{q}(t)$ and $\dot{\boldsymbol{q}}(t)$ are measurable and under the constraint that the spacecraft masses, disturbance forces, and gravitational force are not known precisely [i.e., $\boldsymbol{\theta}$ defined in Eq. (15) is unknown].

The closeness of this control objective is quantified by the position tracking error $\boldsymbol{e}(t) \in \mathbb{R}^3$ defined as

$$\boldsymbol{e}(t) \triangleq \boldsymbol{q}_{\mathrm{d}}(t) - \boldsymbol{q}(t) \tag{16}$$

To account for the system parametric uncertainty, the controller will contain an adaptation law for on-line estimation of the unknown parameters. The difference between the actual and estimated parameters is defined by

$$\tilde{\boldsymbol{\theta}}(t) \triangleq \boldsymbol{\theta} - \hat{\boldsymbol{\theta}}(t) \tag{17}$$

where $\tilde{\boldsymbol{\theta}}(t) \in \mathbb{R}^6$ denotes the parameter estimation error vector and $\hat{\boldsymbol{\theta}}(t) \in \mathbb{R}^6$ denotes the dynamic estimate of the unknown, parameter vector $\boldsymbol{\theta}$. In addition, we define a filtered tracking error, denoted by $\boldsymbol{r}(t) \in \mathbb{R}^3$, as

$$\boldsymbol{r}(t) \triangleq \dot{\boldsymbol{e}}(t) + \Lambda \boldsymbol{e}(t) \tag{18}$$

where $\Lambda \in \mathbb{R}^{3\times 3}$ is a constant, diagonal, positive-definite, control gain matrix. The definition of Eq. (18) will allow us to consider the second-order dynamic equation of Eq. (8) as a first-order equation, thereby simplifying the design/analysis of the controller.

IV. Control Formulation

In the following, we present the complete design and stability analysis of an adaptive controller for the nonlinear, relative position dynamics of MSFF. We initiate the control design by rewriting the dynamics of Eq. (8) in terms of the definition given in Eq. (18). To this end, we differentiate Eq. (18) with respect to time and multiply both sides of the resulting equation by m_{f} to yield

$$m_{\mathrm{f}}\dot{\boldsymbol{r}} = m_{\mathrm{f}}(\ddot{\boldsymbol{q}}_{\mathrm{d}} + \Lambda \dot{\boldsymbol{e}}) - m_{\mathrm{f}}\ddot{\boldsymbol{q}} \tag{19}$$

where we have used the fact derived from Eq. (16) that $\ddot{\boldsymbol{e}} = \ddot{\boldsymbol{q}}_{\mathrm{d}} - \ddot{\boldsymbol{q}}$. After using the system dynamics of Eq. (8) to substitute for $m_{\mathrm{f}}\ddot{\boldsymbol{q}}$ in Eq. (19), we have

$$\begin{aligned} m_{\mathrm{f}}\dot{\boldsymbol{r}} &= m_{\mathrm{f}}(\ddot{\boldsymbol{q}}_{\mathrm{d}} + \Lambda \dot{\boldsymbol{e}}) + C(\omega)\dot{\boldsymbol{q}} + N(\boldsymbol{q}, \omega, \boldsymbol{R}, \boldsymbol{u}_{\ell}) + \boldsymbol{F}_{\mathrm{d}} - \boldsymbol{u}_{\mathrm{f}} \\ &= W(\ddot{\boldsymbol{q}}_{\mathrm{d}} + \Lambda \dot{\boldsymbol{e}}, \dot{\boldsymbol{q}}, \boldsymbol{q}, \omega, \boldsymbol{R}, \boldsymbol{u}_{\ell})\boldsymbol{\theta} - \boldsymbol{u}_{\mathrm{f}} \end{aligned} \tag{20}$$

where Eq. (13) has been used with

$$\boldsymbol{\xi} = \ddot{\boldsymbol{q}}_{\mathrm{d}} + \Lambda \dot{\boldsymbol{e}} \tag{21}$$

in the definition of Eq. (14). The preceding first-order, nonlinear, differential equation represents the open-loop dynamics of $\boldsymbol{r}(t)$ and will be used as the foundation for the synthesis of the adaptive controller.

Based on the form of the open-loop dynamics of Eq. (20), the control input $\boldsymbol{u}_{\mathrm{f}}(t)$ is designed as follows:

$$\boldsymbol{u}_{\mathrm{f}} = W(\cdot)\hat{\boldsymbol{\theta}} + K\boldsymbol{r} \tag{22}$$

where $K \in \mathbb{R}^{3\times 3}$ is a constant, diagonal, positive-definite, control gain matrix. Motivated by the subsequent Lyapunov stability analysis, the parameter estimate vector $\hat{\boldsymbol{\theta}}(t)$ is updated using the adaptation algorithm

$$\dot{\hat{\boldsymbol{\theta}}} = \Gamma W^T(\cdot)\boldsymbol{r} \tag{23}$$

where $\Gamma \in \mathbb{R}^{6\times 6}$ is a constant, diagonal, positive-definite, adaptation gain matrix. Substituting Eq. (22) into Eq. (20) produces the closed-loop dynamics for $\boldsymbol{r}(t)$ as shown next:

$$m_{\mathrm{f}}\dot{\boldsymbol{r}} = -K\boldsymbol{r} + W(\cdot)\tilde{\boldsymbol{\theta}} \tag{24}$$

where the definition of Eq. (17) was used. In addition, by differentiating Eq. (17) with respect to time, we can use Eq. (23) to form the following closed-loop dynamics for the parameter estimation error

$$\dot{\tilde{\boldsymbol{\theta}}} = -\Gamma W^T(\cdot)\boldsymbol{r} \tag{25}$$

The combination of the error systems of Eqs. (24) and (25) gives a stability result for the position and velocity tracking errors as delineated by the following theorem.

Theorem 1: The adaptive control law described by Eqs. (22) and (23) ensures the global asymptotic convergence of the position and velocity tracking errors as illustrated by

$$\lim_{t\to\infty} \boldsymbol{e}(t), \dot{\boldsymbol{e}}(t) = 0 \tag{26}$$

Proof: To prove the preceding result, we define the Lyapunov function

$$V(\boldsymbol{r}, \tilde{\boldsymbol{\theta}}) \triangleq \tfrac{1}{2}\boldsymbol{r}^T m_{\mathrm{f}}\boldsymbol{r} + \tfrac{1}{2}\tilde{\boldsymbol{\theta}}^T\Gamma^{-1}\tilde{\boldsymbol{\theta}} \tag{27}$$

Differentiating Eq. (27) with respect to time yields

$$\dot{V}(\boldsymbol{r}, \tilde{\boldsymbol{\theta}}) = \boldsymbol{r}^T m_{\mathrm{f}}\dot{\boldsymbol{r}} + \tilde{\boldsymbol{\theta}}^T\Gamma^{-1}\dot{\tilde{\boldsymbol{\theta}}} \tag{28}$$

After substituting the closed-loop dynamics of Eq. (24) into Eq. (28), we get

$$\dot{V}(\boldsymbol{r}, \tilde{\boldsymbol{\theta}}) = -\boldsymbol{r}^T K\boldsymbol{r} + \tilde{\boldsymbol{\theta}}^T[W^T(\cdot)\boldsymbol{r} + \Gamma^{-1}\dot{\tilde{\boldsymbol{\theta}}}] \tag{29}$$

Substituting Eq. (25) into the bracketed term simplifies Eq. (29) to

$$\dot{V}(\boldsymbol{r}, \tilde{\boldsymbol{\theta}}) = -\boldsymbol{r}^T K\boldsymbol{r} \le -\lambda_{\min}\{K\}\|\boldsymbol{r}\|^2 \le 0 \tag{30}$$

where $\lambda_{\min}\{\cdot\}$ denotes the minimum eigenvalue of a matrix.

Because of the form of Eq. (30), we know that $V(\boldsymbol{r}, \tilde{\boldsymbol{\theta}})$ is either decreasing or constant. Because $V(\boldsymbol{r}, \tilde{\boldsymbol{\theta}})$ of Eq. (27) is a nonnegative function, we can conclude that $V(\boldsymbol{r}, \tilde{\boldsymbol{\theta}}) \in \mathcal{L}_\infty$; hence, $\boldsymbol{r}(t) \in \mathcal{L}_\infty$, and $\tilde{\boldsymbol{\theta}}(t) \in \mathcal{L}_\infty$. Because $\boldsymbol{r}(t) \in \mathcal{L}_\infty$, we can use Lemma 1.4 of Ref. 12 to show that $\boldsymbol{e}(t), \dot{\boldsymbol{e}}(t) \in \mathcal{L}_\infty$; hence, because of the boundedness of $\boldsymbol{q}_{\mathrm{d}}(t)$ and $\dot{\boldsymbol{q}}_{\mathrm{d}}(t)$, we can use Eq. (16) to conclude that $\boldsymbol{q}(t), \dot{\boldsymbol{q}}(t) \in \mathcal{L}_\infty$. Because $\tilde{\boldsymbol{\theta}}(t) \in \mathcal{L}_\infty$ and $\boldsymbol{\theta}$ is a constant vector, Eq. (17) can be used to show that $\hat{\boldsymbol{\theta}}(t) \in \mathcal{L}_\infty$. From the preceding boundedness statements and the fact that $\ddot{\boldsymbol{q}}_{\mathrm{d}}(t)$ is assumed bounded, the definitions of Eqs. (14) and (21) can be used to state that $W(\cdot) \in \mathcal{L}_\infty$. It is now easy to see from Eq. (22) that the control input $\boldsymbol{u}_{\mathrm{f}}(t) \in \mathcal{L}_\infty$. The preceding information can be applied to Eqs. (8) and (24) to illustrate that $\ddot{\boldsymbol{q}}(t), \dot{\boldsymbol{r}}(t) \in \mathcal{L}_\infty$. Thus, we have explicitly illustrated that all signals in the adaptive controller and system remain bounded during the closed-loop operation.

From Eq. (30) it is now easy to show that $\boldsymbol{r}(t) \in \mathcal{L}_2$. Because we have already proved that $\boldsymbol{r}(t), \dot{\boldsymbol{r}}(t) \in \mathcal{L}_\infty$, we can apply Barbalat's Lemma[12,13] to conclude that

$$\lim_{t\to\infty} \boldsymbol{r}(t) = 0 \tag{31}$$

Finally, Lemma 1.6 of Ref. 12 can be applied to Eqs. (31) and (18) to obtain the result of Eq. (26). □

Remark 2: In the case that the parameter vector $\boldsymbol{\theta}$ of Eq. (15) is perfectly known, the proposed control law (22) with $\hat{\boldsymbol{\theta}} = \boldsymbol{\theta}$ (i.e., an exact model knowledge controller) would ensure global exponential convergence of the position and velocity tracking errors in the sense that

$$\|\boldsymbol{r}(t)\| \le \|\boldsymbol{r}(0)\| \exp\left(-\frac{\lambda_{\min}\{K\}}{m_f}t\right) \tag{32}$$

This result can be proven by defining the Lyapunov function $V \triangleq \frac{1}{2}\boldsymbol{r}^T m_{\mathrm{f}}\boldsymbol{r}$ and using similar arguments as in the proof of Theorem 1 along with Lemma 1.5 of Ref. 12. This stability result improves upon the asymptotic stability result for the position tracking error obtained by the exact model knowledge controllers proposed in Refs. 14 and 15.

Remark 3: To minimize fuel consumption, many MSFF control systems use pulse-type actuators, e.g., Hall thrusters and pulse plasma thrusters[16]; hence, the application of continuous-time control inputs in these cases for long periods of time is not practical as noted in Refs. 3 and 14. This constraint would require the implementation of a pulsed-based version of the proposed nonlinear controller. The effect of this noncontinuous, nonlinear control law on the closed-loop stability has not be considered in this work and constitutes an interesting open problem in MSFF control. However,

as mentioned in Ref. 14, continuous MSFF control laws can provide an idealized system response for comparison purposes with the actual responses obtained from the noncontinuous implementation of the controllers.

Remark 4: The controller just developed was based on a system dynamics that modeled the spacecraft as point masses, i.e., the spacecraft attitude dynamics was neglected. As a result, we only required the design of a translational position controller. A more complete description of MSFF should include not only the attitude dynamics of the spacecraft but also the nonlinear couplings between the translational and attitude dynamics. The resulting six-degree-of-freedom, coupled, nonlinear equations of motion will then dictate the development of a control system where the torque and force inputs must be designed in tandem to accurately control the translation and orientation of the follower spacecraft relative to the leader spacecraft. This issue will be addressed in future work.

V. Simulation Results

The adaptive control law described in the preceding section was simulated for a two spacecraft MSFF problem having the following parameters[3,9]:

$$M = 5.974 \times 10^{24}\ \text{kg}, \qquad m_f = 410\ \text{kg}, \qquad m_\ell = 1550\ \text{kg}$$

$$G = 6.673 \times 10^{-11}\ \text{m}^3/\text{kg}\cdot\text{s}^2, \qquad \boldsymbol{R} = [0, 4.224 \times 10^7, 0]^T\ \text{m}$$

$$\omega = 7.272 \times 10^{-5}\ \text{rad/s}, \qquad \boldsymbol{u}_\ell = 0\ \text{N}$$

$$\boldsymbol{F}_d = [-1.025, 6.248, -2.415] \times 10^{-5}\ \text{N} \tag{33}$$

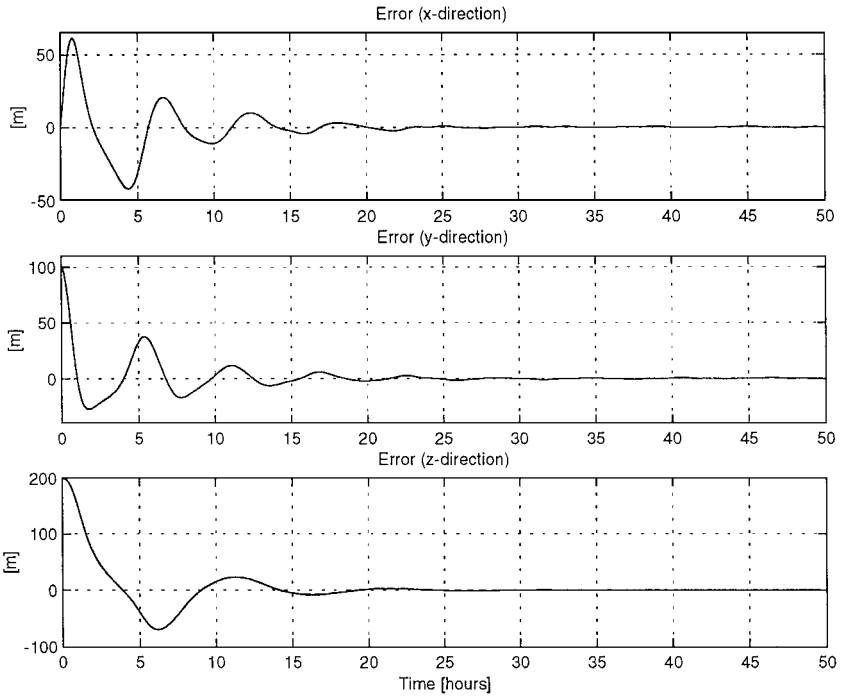

Fig. 2 Position tracking error.

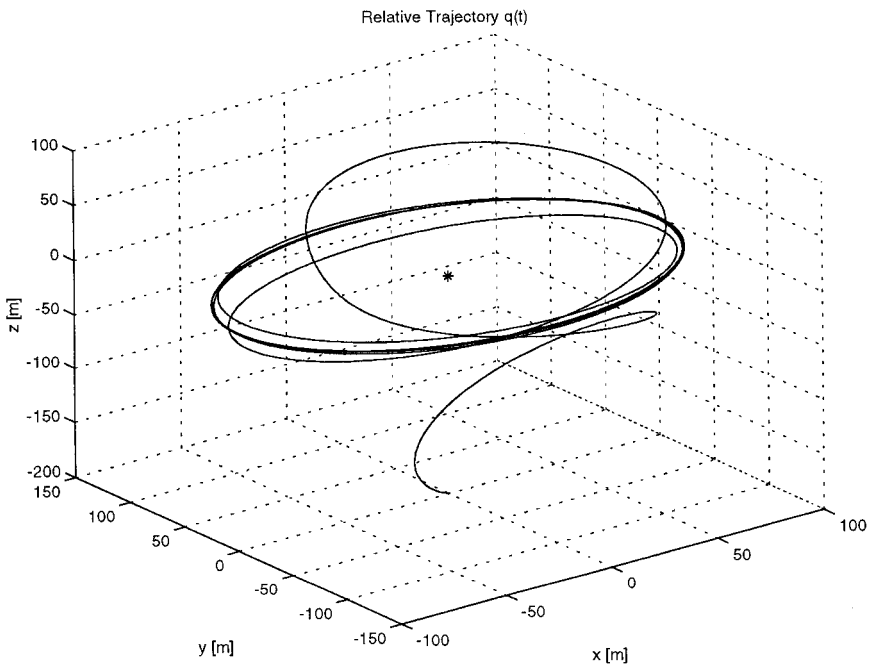

Fig. 3 Actual trajectory $q(t)$ of the follower spacecraft ($*$ denotes the leader spacecraft).

The desired relative trajectory was selected as

$$\boldsymbol{q}_{\mathrm{d}}(t) = \begin{bmatrix} 100\sin(4\omega t)[1-\exp(-0.05t^3)] \\ 100\cos(4\omega t)[1-\exp(-0.05t^3)] \\ 0 \end{bmatrix} \mathrm{m} \qquad (34)$$

where the exponential term was included to ensure that $\dot{\boldsymbol{q}}_{\mathrm{d}}(0) = \ddot{\boldsymbol{q}}_{\mathrm{d}}(0) = 0$. The relative position and relative velocity were initialized to

$$\boldsymbol{q}(0) = [0, 0, -200]^T \mathrm{m}, \qquad \dot{\boldsymbol{q}}(0) = 0\,\mathrm{m/s} \qquad (35)$$

whereas the desired trajectory of Eq. (34) and the initial conditions of Eq. (35) represent a follower spacecraft that is initially stationary with respect to the leader spacecraft and is then commanded to move around the leader spacecraft in a circular orbit of radius 100 m in the $x_\ell - y_\ell$ plane with a constant angular velocity 4ω. The selection of the preceding desired trajectory did not take into account any fuel consumption considerations; however, it illustrates the capability of the proposed controller to track demanding trajectories that may occur during formation reconfiguration maneuvers.

The control and adaptation gains in the following simulation were tuned by trial and error until a good tracking performance was achieved while the parameter estimates were initialized to 50%

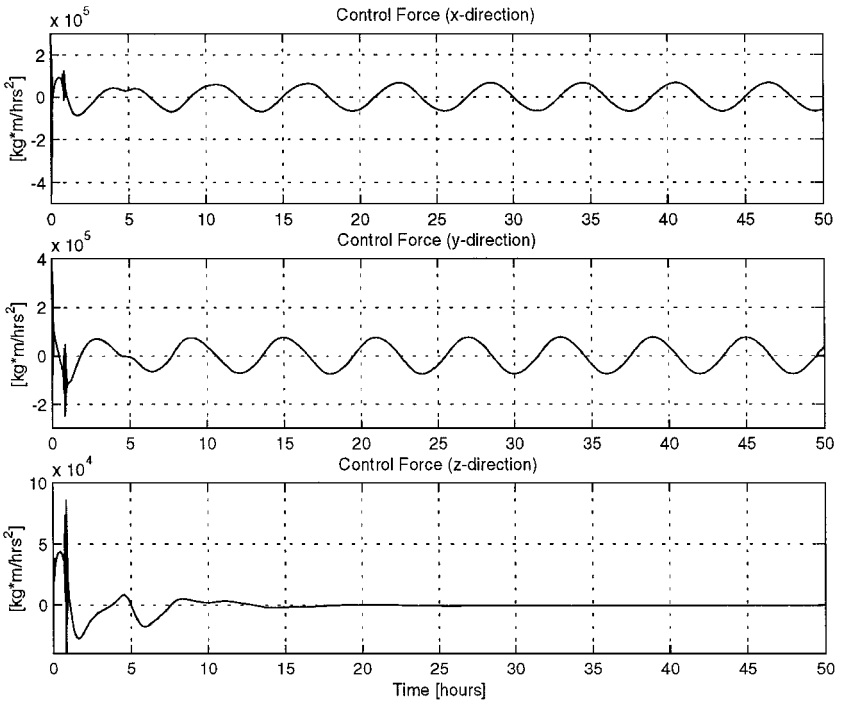

Fig. 4 Control input.

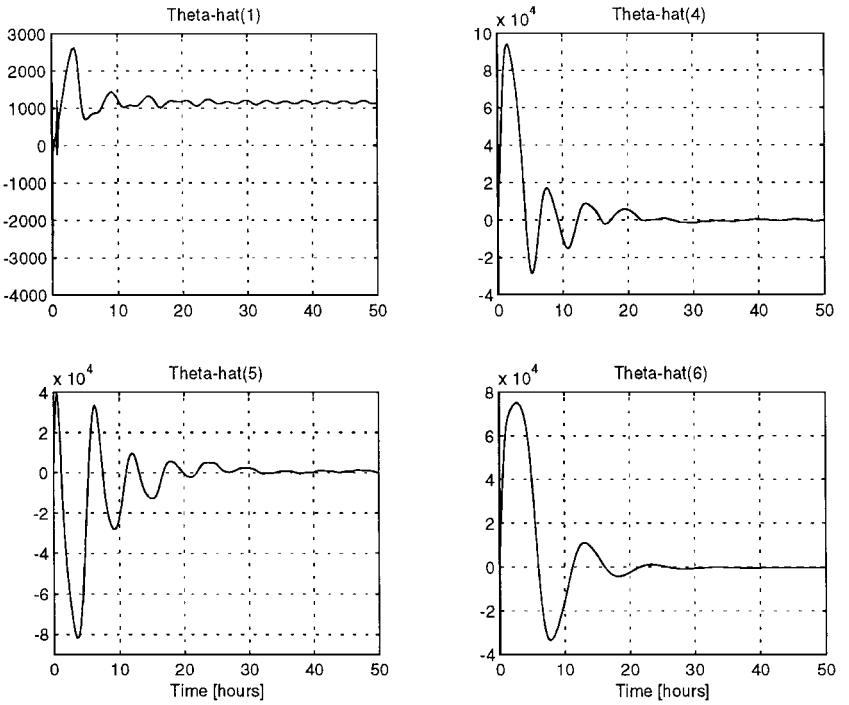

Fig. 5 Sample of parameter estimates.

of the actual parameter values defined in Eqs. (15) and (33) [i.e., $\hat{\theta}(0) = 0.5\theta$]. The set of gains that led to the results shown in Figs. 2–5 are given next:

$$\Lambda = \text{diag}(2, 2, 1), \qquad K = \text{diag}(100, 200, 120)$$

$$\Gamma = \text{diag}(500, 50, 300, 600, 850, 480) \tag{36}$$

Figure 2 depicts the position tracking error $\boldsymbol{e}(t)$. The phase portrait of the trajectory $\boldsymbol{q}(t)$ of the follower spacecraft relative to the leader spacecraft is illustrated in Fig. 3, where $*$ represents the leader spacecraft at the origin. The control input $\boldsymbol{u}_f(t)$ is given in Fig. 4, whereas four components of the parameter estimate vector $\hat{\boldsymbol{\theta}}(t)$ are shown in Fig. 5.

VI. Conclusion

In this paper we presented the development of a nonlinear adaptive control law for the relative position tracking of multiple spacecraft in formation flying. Using a Lyapunov-based design and analysis framework, the proposed controller was shown to guarantee global asymptotic position tracking errors while compensating for unknown spacecraft masses, disturbance forces, and gravity forces. In comparison to previous work, we note that the proposed controller ensures stronger stability results and accounts for a wider class of parametric uncertainties. Simulation results were provided to demonstrate the performance of the controller. Future work will concentrate on the extension of the preceding nonlinear control design framework to other multiple spacecraft formation flying control problems such as position and orientation control, actuator saturation, and output feedback control.

Acknowledgments

This work was supported in part by the Air Force Office of Scientific Research under Grant F49620-93-C-0063, the Air Force Research Lab/VAAD, WPAFB, OH, under IPA: Visiting Faculty Grant, and the NASA/New York Space Grant Consortium under Grant 32310-5891.

References

[1]Bauer, F., Bristow, J., Folta, D., Hartman, K., Quinn, D., and How, J., "Satellite Formation Flying Using an Innovative Autonomous Control System (AUTOCON) Environment," *Proceedings of the AIAA Guidance, Navigation, and Control Conference*, AIAA, Reston, VA, 1997, pp. 657–666.

[2]Robertson, A., Corazzini, T., and How, J. P., "Formation Sensing and Control Technologies for a Separated Spacecraft Interferometer," *Proceedings of the American Control Conference*, Philadelphia, 1998, pp. 1574–1579.

[3]Vassar, R. H., and Sherwood, R. B., "Formationkeeping for a Pair of Satellites in a Circular Orbit," *Journal of Guidance, Control, and Dynamics*, Vol. 8, No. 2, 1985, pp. 235–242.

[4]Redding, D. C., Adams, N. J., and Kubiak, E. T., "Linear-Quadratic Stationkeeping for the STS Orbiter," *Journal of Guidance, Control, and Dynamics*, Vol. 12, No. 2, 1989, pp. 248–255.

[5]Lau, K., Colavita, M., Blackwood, G., Linfield, R., Shao, M., and Gallagher, D., "The New Millenium Formation Flying Optical Interferometer," *Proceedings of the AIAA Guidance, Navigation, and Control Conference*, AIAA, Reston, VA, Aug. 1997, pp. 650–656.

[6]Guinn, J. R., "Autonomous Navigation for the New Millenium Program Earth Orbiter 1 Mission," *Proceedings of the AIAA Guidance, Navigation, and Control Conference*, AIAA, Reston, VA, 1997, pp. 612–617.

[7]Chobotov, V. A. (ed.), *Orbital Mechanics*, AIAA, Reston, VA, 1996, pp. 31–33.

[8]Clohessy, W. H., and Wiltshire, R. S., "Terminal Guidance System for Satellite Rendezvous," *Journal of Aerospace Science*, Vol. 27, No. 9, 1960, pp. 653–658.

[9]Kapila, V., Sparks, A. G., Buffington, J., and Yan, Q., "Spacecraft Formation Flying: Dynamics and Control," *Proceedings of the American Control Conference*, San Diego, CA, 1999, pp. 4137–4141.

[10]Leonard, C. L., Hollister, W. M., and Bergmann, E. V., "Orbital Formationkeeping with Differential Drag," *Journal of Guidance, Control, and Dynamics*, Vol. 12, No. 1, 1989, pp. 108–113.

[11]Hadaegh, F. Y., Lu, W. M., and Wang, P. C., "Adaptive Control of Formation Flying Spacecraft for Interferometry," *International Federation of Automatic Control Conference on Large Scale Systems*, Rio Patras, Greece, 1998, pp. 97–102.

[12]Dawson, D. M., Hu, J., and Burg, T. C., *Nonlinear Control of Electric Machinery*, Marcel Dekker, New York, 1998, pp. 1–19.

[13]Slotine, J. J., and Li, W., *Applied Nonlinear Control*, Prentice–Hall, Upper Saddle River, NJ, 1991, pp. 122–126.

[14]Wang, P. K. C., and Hadaegh, F. Y., "Coordination and Control of Multiple Microspacecraft Moving in Formation," *Journal of Astronautical Sciences*, Vol. 44, No. 3, 1996, pp. 315–355.

[15]Wang, P. K. C., Hadaegh, F. Y., and Lau, K., "Synchronized Formation Rotation and Attitude Control of Multiple Free-Fyling Spacecraft," *Journal of Guidance, Control, and Dynamics*, Vol. 22, No. 1, 1999, pp. 1582–1589.

[16]Schilling, J., and Spores, R., "Comparison of Propulsion Options for TechSat 21 Mission," *Air Force Research Laboratory—Formation Flying and Micro-Propulsion Workshop*, Lancaster, CA, Oct. 1998.